ELSEVIER

Journal of Alloys and Compounds 469 (2009) 146–151

Journal of ALLOYS AND COMPOUNDS

www.elsevier.com/locate/jallcom

An investigation of the high-Al part of the Al–Pd–Ru phase diagram at 790–900 °C

D. Pavlyuchkov [a,b,*], B. Grushko [a], T.Ya. Velikanova [b]

[a] *Institut für Festkörperforschung, Forschungszentrum Jülich, D-52425 Jülich, Germany*
[b] *I.N. Frantsevich Institute for Problems of Materials Science, 03680 Kiev 142, Ukraine*

Received 21 December 2007; received in revised form 27 January 2008; accepted 29 January 2008
Available online 17 March 2008

Abstract

Partial isothermal sections of the Al–Pd–Ru phase diagram at 790 and 900 °C are presented. Complex orthorhombic ε-phases extending from Al_3Pd up to 15 at.% Ru exhibit structural variants including transient irregular structures. The Al_3Pd_2 phase dissolves up to 2 at.% Ru, $Al_{13}Ru_4$ <2.5 at.% Pd and Al_2Ru up to 1 at.% Pd. A stable icosahedral quasicrystalline phase is formed around the $Al_{71.5}Pd_{17}Ru_{12.5}$ composition. At nearby compositions two complex primitive cubic phases with $a \approx 2.0$ and ≈4.0 nm were observed. These cubic phases exhibit powder X-ray diffraction (XRD) patterns very similar to that of the icosahedral phase. At compositions close to the high-Ru limit of the ε-range the electron diffraction patterns of complex orthorhombic structures and 1D quasicrystalline structure were revealed. At lower-Al concentrations three ternary cubic phases structurally related to quasicrystals are formed: primitive C ($a \approx 0.75$ nm), bcc C_1 and fcc C_2 with a double lattice parameter.

Keywords: Intermetallics; X-ray diffraction; Phase diagram

1. Introduction

In this contribution we continue the investigation of the high-Al-range of Al–Pd–Ru reported for the temperature range between 1000 and 1100 °C in Ref. [1]. The previous study revealed the formation of three structurally related cubic phases: C ($Pm\bar{3}$, $a = 0.7757$ nm), C_1 ($Im\bar{3}$, $a = 1.5532$ nm) and C_2 ($Fm\bar{3}$, $a = 1.5566$ nm), and confirmed the formation of a stable icosahedral quasicrystalline phase earlier reported in Ref. [2]. Another complex face-centered cubic structure with $a \approx 3.96$ nm (designated F_{40} in Ref. [1]), closely related to the icosahedral phase (I-phase), was found to be formed at the high-Ru limit of the icosahedral range, which at 1000 °C extended between the $Al_{72.5}Pd_{13}Ru_{14.5}$ and $Al_{70.0}Pd_{19.5}Ru_{10.5}$ compositions. Orthorhombic phases originating from the Al–Pd ε-phases were observed in a ternary range extending from 13 to 15.5 at.% Ru, but were expected to link to the binary terminal at lower temperatures. The $Al_{13}Ru_4$ phase was found to contain less than 2.5 at.% Pd and Al_2Ru up to 1 at.% Pd.

Below we report an investigation of the phase equilibrium in the Al–AlPd–Al_2Ru compositional range and the temperature range of 790–900 °C. The boundary Al–Pd phase diagram is accepted according to Ref. [3] and Al–Ru according to Ref. [4].

2. Experimental

More than 60 alloys were produced from the constituent elements by levitation induction melting in a water-cooled copper crucible under an Ar atmosphere. The purity of Al was 99.999%, of Pd 99.95% and of Ru 99.9%. Considering the high price of the components the ingots were typically of about 3 g. It is difficult to dissolve Ru in Al. Therefore, more homogeneous alloys were prepared using Ru powder which was first mechanically compressed with Pd powder into pellets and then melted together with Al. In addition, due to the high-temperature peritectic formation of the phases in Al–Ru and ternary compositions significant segregation occurred during solidification. The final ingots were quite inhomogeneous. The ingots were broken and their parts were treated as individual samples.

Parts of the samples were annealed under an Ar atmosphere or vacuum for times depending on the annealing temperature. Due to sluggish reaction kinetics the annealing time at 790 °C was up to 4500 h, at 900 °C up to 836 h.

Single-phase samples were selected using powder X-ray diffraction (XRD) and scanning electron microscopy (SEM). Their compositions were examined by inductively coupled plasma optical emission spectroscopy (ICP-OES) and

* Corresponding author at: Institut für Festkörperforschung, Forschungszentrum Jülich, D-52425 Jülich, Germany. Tel.: +49 2461 614693; fax: +49 2461 616444.
E-mail addresses: d.pavlyuchkov@fz-juelich.de, d.pavlyuchkov@googlemail.com (D. Pavlyuchkov).

0925-8388/$ – see front matter © 2008 Elsevier B.V. All rights reserved.
doi:10.1016/j.jallcom.2008.01.138

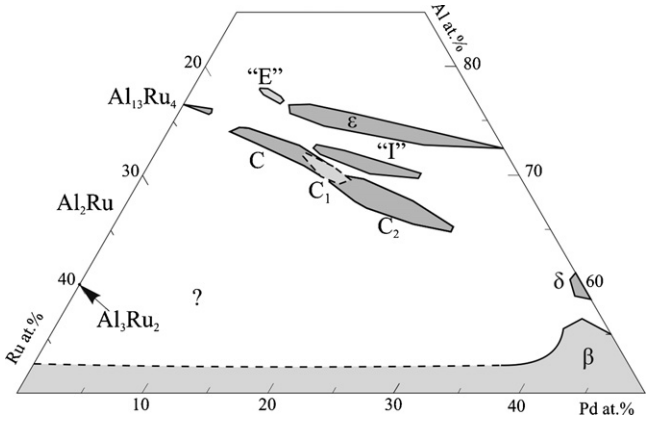

Fig. 1. Projection of overall compositions of the phases in the high-Al part of Al–Pd–Ru.

by energy-dispersive X-ray analysis (EDX) in SEM. Powder XRD was carried out in the transmission mode using Cu $K\alpha_1$ radiation and a position-sensitive detector. The samples were also studied by electron diffraction in the transmission electron microscopes (TEM) JEOL FX 4000 and Philips CM 200 operated at 400 and 200 kV, respectively. The TEM samples were powders spread on Cu grids covered by carbon films. The melting temperatures of the phases were determined by differential thermal analysis (DTA) at rates of 5–20 °C/min.

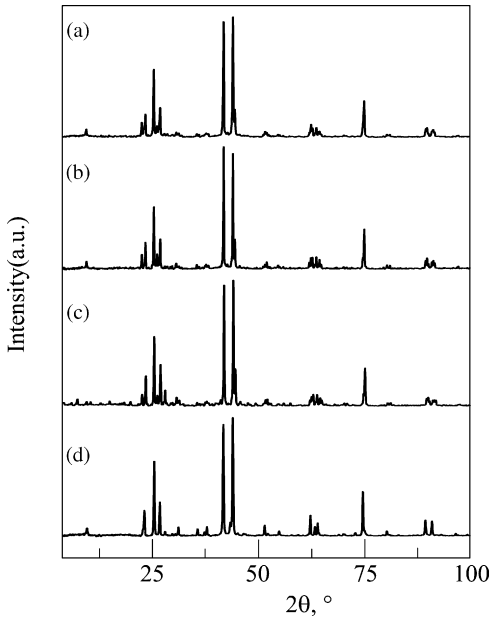

Fig. 2. Powder XRD patterns (Cu $K\alpha_1$ radiation) of the: (a) I-phase, (b) F_{40}-phase [1], (c) P_{40}, and (d) P_{20}.

3. Results and discussion

3.1. Phases

Three ternary cubic phases C, C_1 and C_2, and the icosahedral I-phase reported in Ref. [1] were also revealed at lower temperatures. Their ranges at 900 and 790 °C specified in the isothermal sections (see below) were somewhat different from those at the higher temperatures. As expected, the ternary ε-range achieved the Al–Pd terminal with decreasing temperature. Apart from this, the Al–Pd δ-phase is formed by a peritectic reaction. The overall compositional ranges of the binary and ternary phases shown in Fig. 1 combine the results of the present study and those in Ref. [1]. The crystallographic data of the phases are included in Table 1.

The binary M–$Al_{13}Ru_4$ and Al_2Ru phases were found to dissolve only a little of the Pd: $Al_{13}Ru_4$ <2.5 at.% and Al_2Ru up to 1 at.%. The Al–Pd δ-phase can dissolve up to 2 at.% Ru. The Al_6Ru phase, whose melting temperature in the binary system is 734 °C [4], was not observed in ternary alloys. Nor did we observe the $Al_{21}Pd_8$ (γ) and Al_4Pd (λ) phases forming in Al–Pd by solid-state reactions [3]. Although their formation temperatures in Al–Pd are considerably below those applied in the present study, these temperatures could increase with increasing concentration of Ru as in the case of the ε-phases. Indeed, in Al–Pd–Ir the λ-phase was stabilized up to 871 °C by disso-

Table 1
Crystallographic data of the Al–Pd–Ru phases mentioned in the text

Phase	S.G. or symmetry	Lattice parameters				For composition
		a (nm)	*b* (nm)	*c* (nm)	*β* (°)	
M–$Al_{13}Ru_4$	*C2/m*	1.5862	0.8188	1.2736	107.77	
Al_2Ru	*Fddd*	0.8012	0.4717	0.8785		
Al_3Ru_2	*I4/mmm*	0.3079	–	1.4330		
ε	Orthorhombic	2.35	1.68	Var.[a]	–	
δ (Al_3Pd_2)	$P\bar{3}m1$	0.42265	–	0.5163	–	
β (AlPd)	$Pm\bar{3}m$	0.3036	–	–	–	
C	$Pm\bar{3}$	0.77568(3)	–	–	–	$Al_{74.5}Pd_{5.0}Ru_{20.0}$
C_1	$Im\bar{3}$	1.55230(17)	–	–	–	$Al_{71}Pd_{13}Ru_{16}$
C_2	$Fm\bar{3}$	1.55659(2)	–	–	–	$Al_{67.7}Pd_{19.7}Ru_{12.6}$
P_{40}	$Pa\bar{3}$	4.0445(7)	–	–	–	$Al_{72.6}Pd_{13.0}Ru_{14.4}$
P_{20}	Cubic	2.0227(5)	–	–	–	$Al_{70.0}Pd_{22.3}Ru_{7.7}$
E_1	Orthorhombic	6.12	1.68	2.00	–	
E_2	Orthorhombic	3.84	1.68	2.0	–	
E_3	Orthorhombic	3.86	1.68	12.6	–	

The lattice parameters are given for the compositions indicated.

[a] The structural variants designated ε_6 and ε_{28}, typical of binary Al–Pd, have $c \approx 1.23$ and ≈5.70 nm, respectively [3], in regular ε_{16} $c \approx 3.24$ nm. A transient structure observed around $Al_{76.5}Pd_{8.5}Ru_{15}$ resembles ε_{16} but several reflections were split.

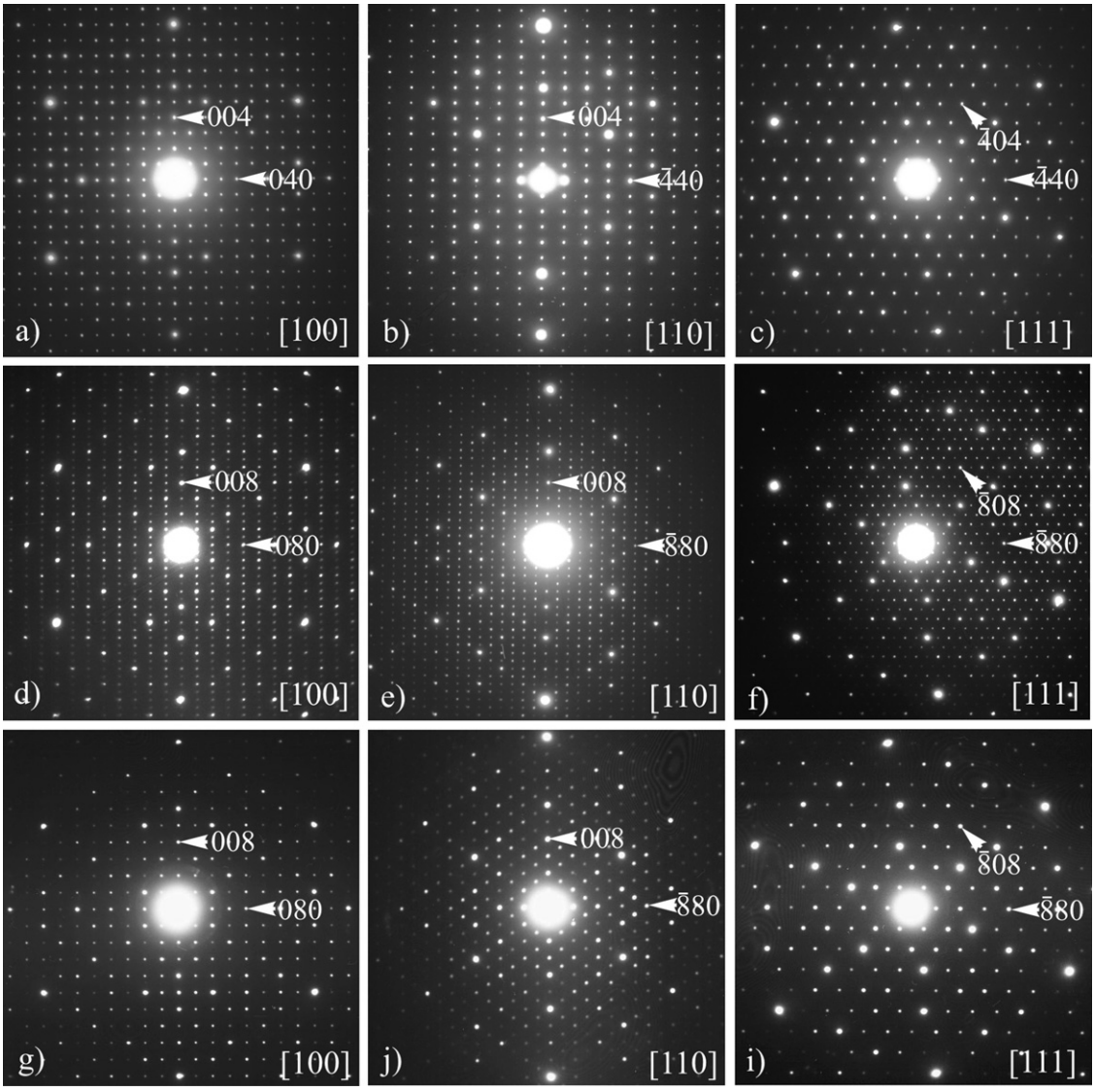

Fig. 3. Electron diffraction patterns of the: (a–c) P_{20}-phase, (d–f) P_{40}-phase and (g–i) F_{40}-phase [1] along the [1 0 0], [1 1 0], and [1 1 1] zone axes.

lution of 15.5 at.% Ir [5]. The dissolution of Ru in this phase is probably much lower than that of Ir.

Around the $Al_{76}Pd_{8.5}Ru_{15.5}$ composition, i.e. close to the high-Ru limit of the ε-range, the ε_{16} structure was revealed by electron diffraction. This result is similar to that in Al–Pd–Fe, but the maximal solubility of Fe in ε is only 10 at.% vs. 15 at.% Ru. At intermediate compositions ε_{22} and transient irregular structures [13] were observed. Other complex structures were observed at even more extended compositions (up to $Al_{77.7}Pd_{5.5}Ru_{16.8}$, see below).

The thermodynamic stability of the ternary I-phase was also confirmed at 900 and 790 °C by long-term annealing. At lower temperatures it was not possible to achieve equilibration for a reasonable time. No complex fcc phase structurally related to the I-phase and forming at 1000 °C at close compositions [1] was observed at 900 or 790 °C. Instead of this so-called F_{40} structure, a primitive structure with essentially the same lattice parameter (P_{40}) is formed at these temperatures at the high-Ru margin of the I-region (see below). Apart from this, an additional complicated primitive cubic structure P_{20} with a lattice parameter $a \approx 2.0$ nm, i.e. half as large as of P_{40}, was revealed at the high-Pd margin of the I-region (see below). While the powder X-ray diffraction patterns of the P_{20}, P_{40}, F_{40} and I phases were almost identical (see Fig. 2), our electron diffraction examinations revealed either icosahedral or periodic essentially single-phase structures (see typical examples in Fig. 3). Some differences can also be seen by close inspection of the powder XRD patterns of the I, P_{40} and P_{20} phases, while those of F_{40} and P_{40} obtained in our experiments were below the level of noise. In Fig. 4 which presents extended parts of the diffraction patterns of Fig. 2, the specific reflections of the P_{20} phase are marked by arrows.

The thermodynamic stability of the P_{20} phase is still unclear although it was observed in the samples annealed for long times at 900 and 790 °C. Such a structure was already described in Ref. [6]. A structure similar to that of P_{20} was also reported to be observed in Al–Pd–Mn, for example in

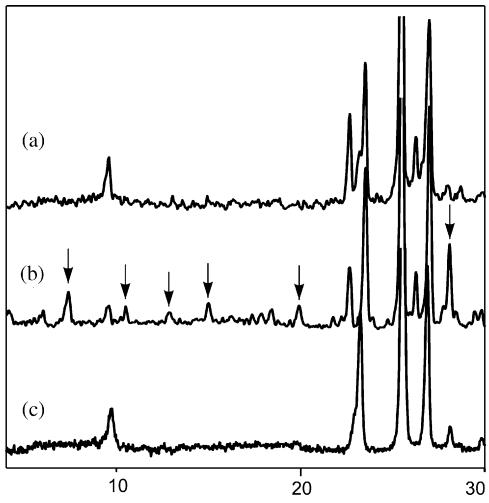

Fig. 4. Details of the powder XRD patterns of the I-phase and related cubic phases shown in Fig. 2: (a) P_{40} and F_{40}, (b) P_{20}, (c) I. The specific reflections of the P_{20}-phase are marked by arrows.

an $Al_{70}Pd_{20}Mn_{10}$ alloy annealed for 3 days at 800 °C [7],[1] or in Al–Pd–Mn–Si [10]. In Ref. [10] a structural model of this phase ($Pm\bar{3}$, $a = 2.0211(2)$ nm) was determined for the $Al_{69.5}Pd_{23.0}Mn_{6.2}Si_{1.3}$ composition using the single-crystal technique. The model includes only Al, Pd and Mn atoms although the studied sample also contained Si. Applying this model, we simulated the powder X-ray diffraction pattern of P_{20} and with the help of these calculations indexed our experimental diffraction pattern (see Table 2). The refined lattice parameter was $a = 2.0227(5)$ nm for the $Al_{70.0}Pd_{22.3}Ru_{7.7}$ composition.

The primitive P_{40} structure with $a \approx 4.0$ nm was observed at 900 and 790 °C between the $Al_{71.5}Pd_{17}Ru_{11.5}$ and $Al_{73}Pd_{11.5}Ru_{15.5}$ compositions. The electron diffraction patterns of the P_{40} phase along the [1 0 0], [1 1 0], and [1 1 1] zone axes are presented in Fig. 3d–f. They show the regular extinctions $k = 2n + 1$ for $0\,k\,l$ and $h = 2n + 1$ for $h\,0\,0$ (h, k, l are cyclically permutable) typical of the $Pa\bar{3}$ space group (No. 205). In contrast, the F_{40}-phase of essentially the same lattice parameter exhibits the ($h + k$, $k + l$, $l + h = 2n$) reflection conditions typical of a face-centered structure (Fig. 3g–i). Direct indexing of the powder XRD patterns of these phases would be quite ambiguous, but we suggested their close structural similarity to P_{20} and assigned double indexes to the strong reflections of F_{40} and P_{40} located at very close 2θ positions to the strong reflections of P_{20}. The refined lattice parameter of P_{40} was 4.0445(7) nm for the $Al_{72.6}Pd_{13.0}Ru_{14.4}$ composition. The lattice parameter of the F_{40} structure observed at the same composition at 1000 °C was also refined and was found to be essentially the same.

Due to the similarity of their powder XRD patterns, the coexistence of the I, P_{20} and P_{40} structures cannot be detected by X-ray diffractometry. Using SEM/EDX we were also unable to detect any compositional gaps between the assumed single-phase regions. Therefore, the I, P_{20} and P_{40} structures are shown as one region designated "I-region" (see Fig. 1). The observation of an ordered structure at higher temperatures and of a disordered structure at lower temperatures is not in favor of their thermodynamic stability. Although both structures were revealed in samples annealed for long time, we cannot exclude that due to sluggish kinetics an intermediate periodic structure is formed and its additional ordering is only achieved at higher temperatures. Such effects have already been reported for other alloy systems in the ranges where quasicrystalline phases are formed at higher temperatures and closely related periodic structures at lower temperatures (see examples in Al–Ni–Co [11,12]).

In contrast to the ε-region, where with compositional variations one orthorhombic structure could continuously convert to another orthorhombic structure via one-dimensional-aperiodic states [13], no transition states between the icosahedral and cubic structures were revealed in the "I"-region. The continu-

Table 2
Powder XRD data of the P_{20}-phase of the $Al_{70.0}Pd_{22.3}Ru_{7.7}$ composition ($a = 2.0227(5)$ nm, $V = 8.2757(33)$ nm^3)

No.	h	k	l	d^{obs}	d^{calc}	$I/I_0{}^{obs}$
1	1	0	0	2.04597	2.02271	3
2	1	1	0	1.43582	1.43027	3
3	1	1	1	1.17367	1.16781	5
4	2	1	0	0.91252	0.90459	3
5	2	1	1	0.83072	0.82577	3
6	2	2	2	0.58488	0.58391	4
7	4	1	1	0.47796	0.47676	3
8	4	2	1	0.44239	0.44139	3
9	3	3	3	0.38959	0.38927	9
10	5	2	0	0.37566	0.37561	24
11	3	5	0	0.34702	0.34689	55
12	6	0	0	0.33727	0.33712	8
13	5	3	2	0.32826	0.32813	33
14	6	2	0	0.31950	0.31982	3
15	5	4	0	0.31582	0.31589	12
16	6	3	0	0.30151	0.30153	3
17	6	3	1	0.29799	0.29823	3
18	3	6	2	0.28891	0.28896	7
19	5	5	1	0.28308	0.28324	4
20	6	5	2	0.25080	0.25089	3
21	8	2	2	0.23808	0.23838	3
22	8	3	0	0.23642	0.23674	4
23	6	7	1	0.21810	0.21811	5
24	5	8	0	0.21430	0.21441	95
25	8	5	3	0.20420	0.20433	100
26	10	0	0	0.20214	0.20227	29
27	5	8	4	0.19723	0.19740	4
28	3	10	2	0.19024	0.19028	3
29	8	8	2	0.17594	0.17605	5
30	5	10	3	0.17467	0.17474	5
31	11	8	0	0.14868	0.14871	5
32	13	3	3	0.14785	0.14792	7
33	8	10	5	0.14708	0.14713	9
34	8	8	8	0.14590	0.14598	3
35	13	5	0	0.14520	0.14522	9
36	5	13	2	0.14374	0.14375	7
37	10	10	0	0.14302	0.14303	5
38	13	8	5	0.12597	0.12593	30
39	10	13	5	0.11809	0.11797	3
40	8	16	5	0.10898	0.10890	6
41	13	13	3	0.10866	0.10859	7

[1] This structure might be metastable. It was not revealed in either Ref. [8] or [9], where relevant alloys were studied after prolonged annealing at comparable temperatures. This phase was not included in the corresponding equilibrium phase diagrams in [8,9].

ity of the region of the genuine icosahedral phase (including the metastable region extending from the binary Al–Ru terminal) implies the possibility of its formation also at compositions where the P_{40} and F_{40} structures were observed. For these compositions the I-phase could appear at still higher temperatures if the melting were suppressed. Indeed, the annealing resulting in the formation of the F_{40} structure was only 80 °C below the solidus, which does not leave much room for a higher temperature solid phase. DTA of the corresponding samples did not reveal any thermal effect which could be associated with a phase transition below that of the melting.

At compositions close to the high-Ru limit of the ε-range the SEM/EDX, electron diffraction and HRTEM examinations revealed new complex orthorhombic structures. No such compositions were measured in as-cast materials, implying the formation of an additional solid phase during annealing at 790–900 °C. On the other hand, we cannot definitely associate the structures observed in TEM at room temperature with those existing at the annealing temperatures. Indeed, inside macroscopic grains of several microns in diameter coherent nano-scaled domains with the parallel *b*-axes were found to be formed. This might be a high-temperature phase transformed during cooling. In the plane perpendicular to the *b*-axes the overall symmetry of the diffraction patterns taken from the grains is pseudo-tenfold. The *b* lattice parameter of these structures, designated E_i in the following, is the same as that of the ε-phases, which is also typical of the decagonal D_4 structure observed in Al–TM alloy systems [14]. In contrast, their other lattice parameters do not follow those typical of the ε-phases sequences described in Ref. [13], and the tiling of their HRTEM images reveals that they are built from clusters which are τ times larger than those typical of the ε-phases. Moreover, the E-structures were revealed at temperatures lower than those of the high-Ru ε-phases. The association of their compositions with the ε-range means that the tendency to increase the existence temperature of the ε-phase with increasing Ru concentration changes to a tendency to decrease after reaching a maximum at 15 at.%. Such decrease was not observed in either of the Al–Pd–TM alloy systems containing ε (see Ref. [14] and references therein).[2] Therefore we present the E-structures as a separate phase range. Close examination revealed a compositional gap of 1 at.% between this range and the ε-range at 790 °C, while no visible compositional differences were revealed at 900 °C. A more detailed structural analysis of these findings will be published elsewhere.

3.2. Isothermal sections

The partial isothermal section at 900 °C is presented in Fig. 5. At this temperature the δ-phase is already solid and dissolves 1 at.% of Ru. The limits of the Pd solubility in the M–$Al_{13}Ru_4$

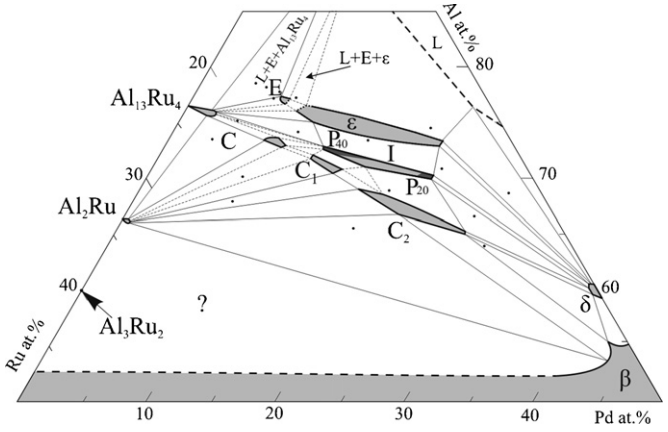

Fig. 5. Partial isothermal section of Al–Pd–Ru at 900 °C. The compositions of the studied alloys are marked by spots, the provisional lines are shown by dotted lines. The liquid is designated L, M–$Al_{13}Ru_4$ is M.

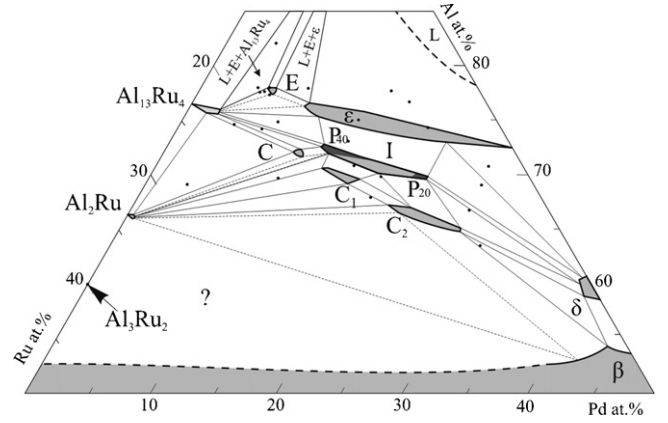

Fig. 6. Partial isothermal section of Al–Pd–Ru at 790 °C. The compositions of the studied alloys are marked by spots, the provisional lines are shown by dotted lines. The liquid is designated L, M–$Al_{13}Ru_4$ is M.

and Al_2Ru phases did not change as compared to those at 1000 °C [1]. The high-Pd limit of the ε-range shifts towards Al–Pd up to $Al_{72,5}Pd_{21}Ru_{6,5}$, while its high-Ru limit remains at the $Al_{77}Pd_{7.5}Ru_{15.5}$ composition. The high-Ru edge the C-region shifts to the $Al_{74}Pd_7Ru_{19}$ composition while the low-Ru edge of the C_1-region is located at $Al_{70.5}Pd_{14.5}Ru_{15}$. The compositional gap between the C and C_1 phases was not detected. This gap and that between the ε and E regions are shown tentatively. The composition of the C_2-phase ranges from $Al_{69}Pd_{17}Ru_{14}$ to $Al_{65.5}Pd_{27}Ru_{7.5}$. The I-range (included P_{40}, I and P_{20}) extends between the compositions $Al_{73}Pd_{11.5}Ru_{15.5}$ and $Al_{70}Pd_{22}Ru_8$. The ε–M–C, L–ε–δ, P–C_2–δ and C_2–δ–β three-phase equilibria are shown on the basis of the results obtained from the investigation of two-phase samples. The C–C_1–Al_2Ru, "I"–C–C_1 and "I"–C_1–C_2 triangles are provisional.

The phase equilibria at 790 °C are shown in Fig. 6. The solubility of Pd in Al–Ru binary phases is not different from that at 900 °C. The solubility of Ru in the δ-phase increases up to 2 at.%. The C_1-region shifts toward slightly lower Al concentrations and occupies a region between $Al_{70.5}Pd_{13}Ru_{26.5}$ and $Al_{69}Pd_{17}Ru_{14}$. The C_2-phase is formed

[2] While in Al–Pd–Rh the ε-range extends from one binary terminal to the other [14], in Al–Pd–Ir only ∼4 at.% separates it from the Al–Ir terminal [5]. It is thus plausible to suggest that in Al–Ir and Al–Ru the ε-phases are only metastable. In this case, the tendency to increase the existence temperature would exist in the whole compositional range as in Al–Pd–Rh.

between $Al_{67.5}Pd_{20}Ru_{12.5}$ and $Al_{65}Pd_{27}Ru_8$. The "I"-region is located at approximately the same compositions as at 900 °C.

The shrinkage of the C-range with decreasing temperature might be an indication of its thermodynamic instability at still lower temperatures. Indeed, the C-phase is only a high-temperature phase in Al–Pd–Fe [3], Al–Ni–Ru [5] and several other alloy systems (see references in Ref. [1]). Therefore the three-phase equilibrium would be expected at lower temperatures between Al_2Ru, $Al_{13}Ru_4$ and a phase from the I-range.

At 790 °C the ε-region is already connected to the Al–Pd terminal. The E-region is formed around $Al_{77.7}Pd_{5.5}Ru_{16.8}$. The L–E–ε, E–ε–M, C_1–Al_2Ru–C_2, Al_2Ru–C_2–β, ε–P_{20}–δ, P_{20}–C_2–δ three-phase equilibria are shown on the basis of results obtained from the investigation of two-phase samples, "I"–C–Al_2Ru and "I"–C_1–C_2 are provisional.

4. Conclusions

Phase equilibria in the Al–Pd–Ru alloy system were studied at 900 and 790 °C in the compositional range above 50 at.% Al.

Binary M–$Al_{13}Ru_4$ was found to dissolve up to 2.5 at.% Pd and Al_2Ru up to 1 at.% Pd. The Al–Pd δ-phase can dissolve up to 2 at.% Ru. The range of the Al–Pd ε-phases was found to extend up to 15 at.% Ru.

Complex ternary cubic phases C, C_1 and C_2 earlier reported in Ref. [1] were also revealed at the temperatures studied. The shrinkage of the C-range with decreasing temperature might be an indication of its thermodynamic instability at still lower temperatures.

Thermal stability of the icosahedral phase was also confirmed at the temperatures studied. A primitive cubic P_{40}-phase with lattice parameter $a \approx 4.0$ nm was found to be formed at the high-Ru margin of the I-region. Also a primitive cubic P_{20}-phase with a lattice parameter half as small was revealed at the high-Pd margin of the I-region. No transition states between the icosahedral structure and these cubic structures related to it were observed.

At compositions close to the high-Ru limit of the ε-range a series of new complex orthorhombic structures was revealed.

Acknowledgements

We thank W. Reichert and M. Schmidt for technical contributions and S. Balanetskyy, M. Yurechko and S. Mi for helpful discussions.

References

[1] D. Pavlyuchkov, B. Grushko, T.Ya. Velikanova, J. Alloy Compd 464 (2008) 101–106.
[2] T. Asao, R. Tamura, S. Takeuchi, Philos. Mag. Lett. 82 (2002) 217.
[3] M. Yurechko, A. Fattah, T. Velikanova, B. Grushko, J. Alloys Compd. 329 (2001) 173.
[4] S. Mi, S. Balanetskyy, B. Grushko, Intermetallics 11 (2003) 643.
[5] D. Pavlyuchkov, B. Grushko, T. Velikanova, J. Alloys Compd. 453 (2008) 191.
[6] T. Shibuya, T. Asao, M. Tamura, R. Tamura, S. Takeuchi, Mater. Sci. Eng. A294–296 (2000) 61.
[7] H.L. Li, K.H. Kuo, Philos. Mag. Lett. 70 (1994) 55.
[8] B. Grushko, M. Yurechko, N. Tamura, J. Alloys Compd. 290 (1999) 164.
[9] S. Balanetskyy, G. Meisterernst, M. Heggen, M. Feuerbacher, Intermetallics 16 (2008) 71.
[10] K. Sugiyama, N. Kaji, K. Hiraga, Z. Kristal. 213 (1998) 90.
[11] B. Grushko, D. Holland-Moritz, R. Wittmann, G. Wilde, J. Alloys Compd. 280 (1998) 215.
[12] B. Grushko, M. Döblinger, Z. Kristal. 219 (2004) 447.
[13] S. Balanetskyy, B. Grushko, T. Velikanova, Z. Kristal. 219 (2004) 548.
[14] B. Grushko, T.Ya. Velikanova, CALPHAD 31 (2007) 217.